Abstract: 074

Inclusive D^* Meson and Associated Dijet Production in Deep-Inelastic Scattering

H1 Collaboration

Abstract

The inclusive production of $D^{*\pm}$ mesons in deep inelastic scattering is studied with the H1 detector at HERA using an integrated luminosity of $47.0\mathrm{pb}^{-1}$. In the kinematic region $2 \leq Q^2 \leq 100$ GeV^2 and $0.05 \leq y \leq 0.7$ an e^+p cross section for inclusive $D^{*\pm}$ meson production of $7.72 \pm 0.23\,(\mathrm{stat.}) \pm 1.09\,(\mathrm{syst.})$ is measured in the visible range $1.5 \leq p_{t,D^*} \leq 15$ GeV and $|\eta_{D^*}| \leq 1.5$. Single and double differential inclusive $D^{*\pm}$ meson cross sections are compared to perturbative calculations in the framework of the DGLAP and CCFM evolution schemes. For events containing a $D^{*\pm}$ meson, the additional requirement of at least two jets with $E_{t,\text{ jet 1}} \geq 4$ GeV, $E_{t,\text{ jet 2}} \geq 3$ GeV and $-1 \leq \eta_{\text{lab, jet 1,2}} \leq 2.5$ is applied. In this kinematic range the inclusive cross section for dijet production associated with a $D^{*\pm}$ meson is found to be $1.63 \pm 0.10\,(\mathrm{stat.}) \pm 0.25\,(\mathrm{syst.})\,\mathrm{nb}$. Differential cross sections for dijet events with $D^{*\pm}$ mesons are also presented and compared to QCD model predictions.

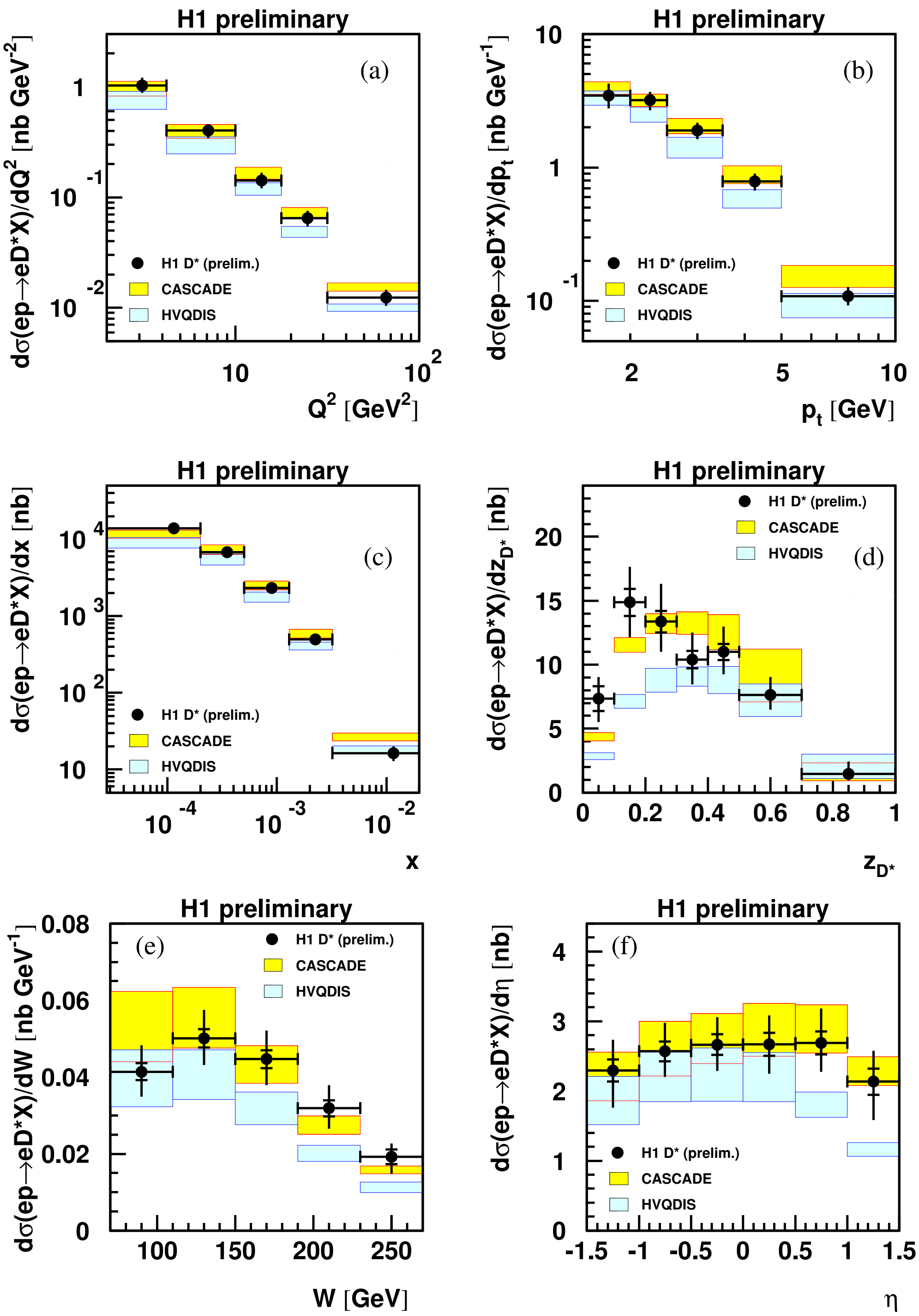

Figure 1: Single differential inclusive cross section $\sigma(ep \to eD^{*\pm}X)$ versus W, x, Q^2 and $p_{t\,D^*}$, η_{D^*}, z_{D^*}. The inner and outer error bars correspond to the statistical and the total errors. The expectation of the NLO DGLAP calculation using HVQDIS with CTEQ5F3 parton densities is indicated by the lower shaded band. The upper shaded band is the expectation of the CCFM calculation based on the CASCADE program with the initial gluon distribution fitted to the inclusive F_2 data. The upper and lower bounds of both calculations correspond to (m_c = 1.3 GeV, $\epsilon_c = 0.035$) and ($m_c = 1.5$ GeV, $\epsilon_c = 0.10$), respectively.

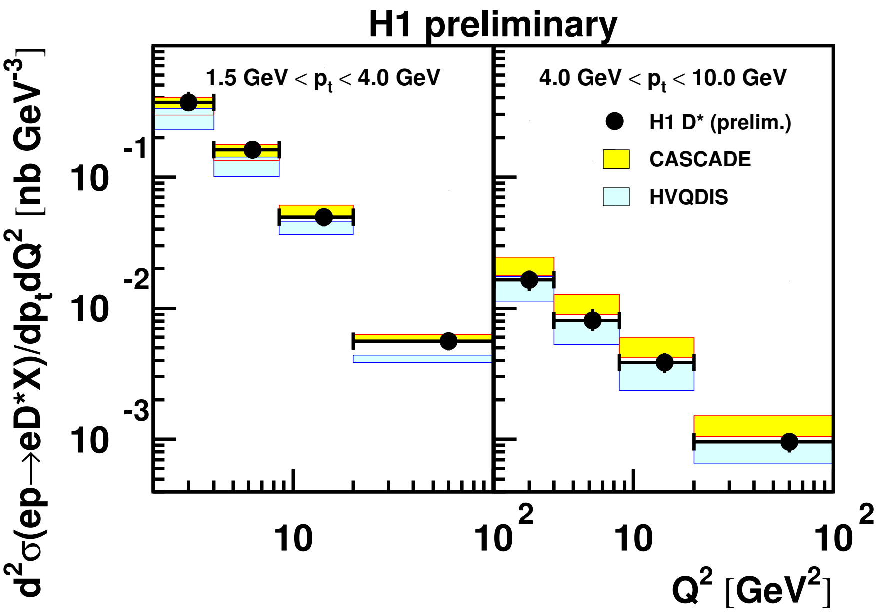

Figure 2: Double differential inclusive cross section $\mathrm{d}^2\sigma/\mathrm{d}p_{t\,D^*}\mathrm{d}Q^2$ in bins of $p_{t\,D^*}$. The inner and outer error bars correspond to the statistical and the total errors. The expectations of the NLO DGLAP calculation using HVQDIS and of the CCFM calculation based on the CASCADE program are also indicated (see figure 1 for details).

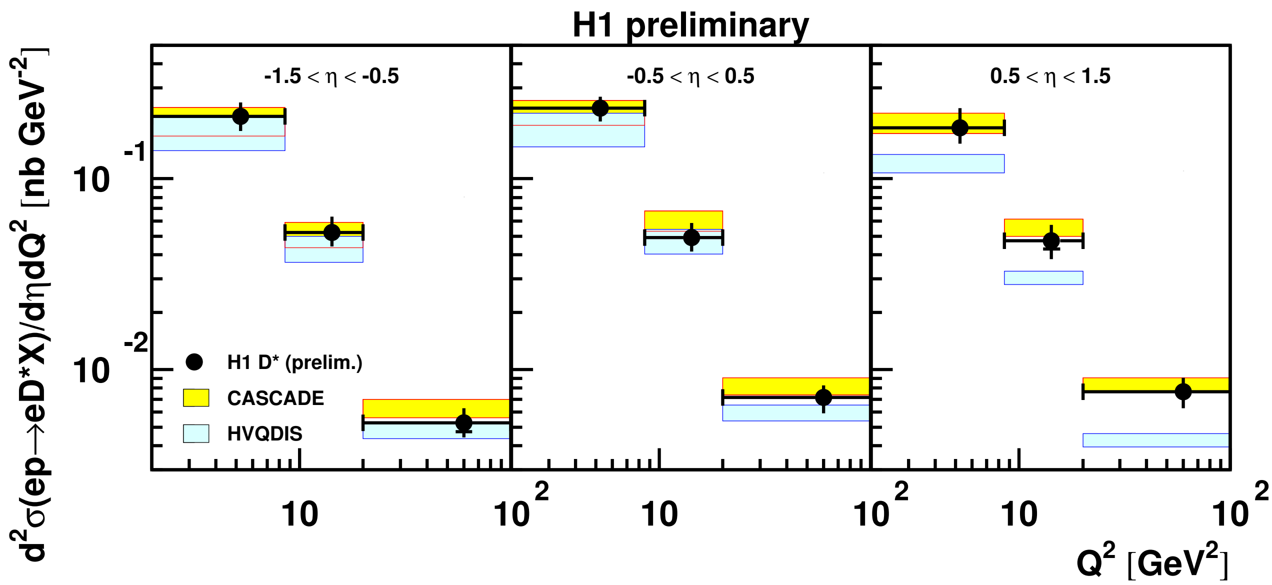

Figure 3: Double differential inclusive cross section $\mathrm{d}^2\sigma/\mathrm{d}\eta_{D^*}\mathrm{d}Q^2$ in bins of η_{D^*}. The inner and outer error bars correspond to the statistical and the total errors. The data are compared to the expectations of the NLO DGLAP calculation using HVQDIS and of the CCFM calculation based on the CASCADE program (see figure 1 for details).

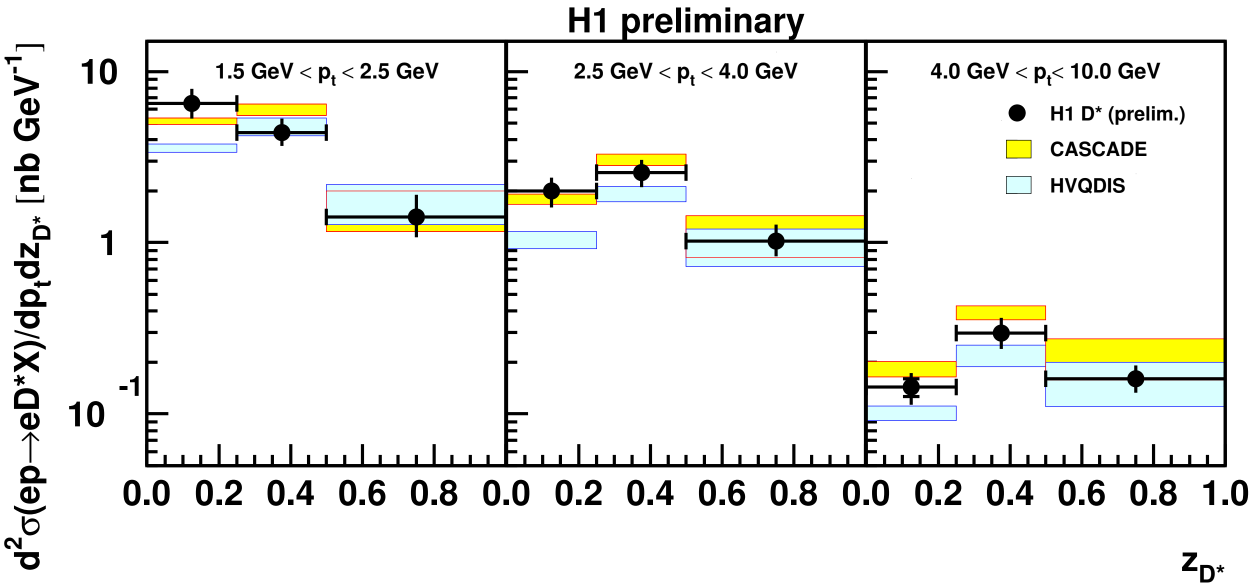

Figure 4: Double differential inclusive cross section $\mathrm{d}^2\sigma/\mathrm{d}p_{t\,D^*}\mathrm{d}z_{D^*}$ in bins of $p_{t\,D^*}$. The inner and outer error bars correspond to the statistical and the total errors. The data are compared to the expectations of the NLO DGLAP calculation using HVQDIS and of the CCFM calculation based on the CASCADE program (see figure 1 for details).

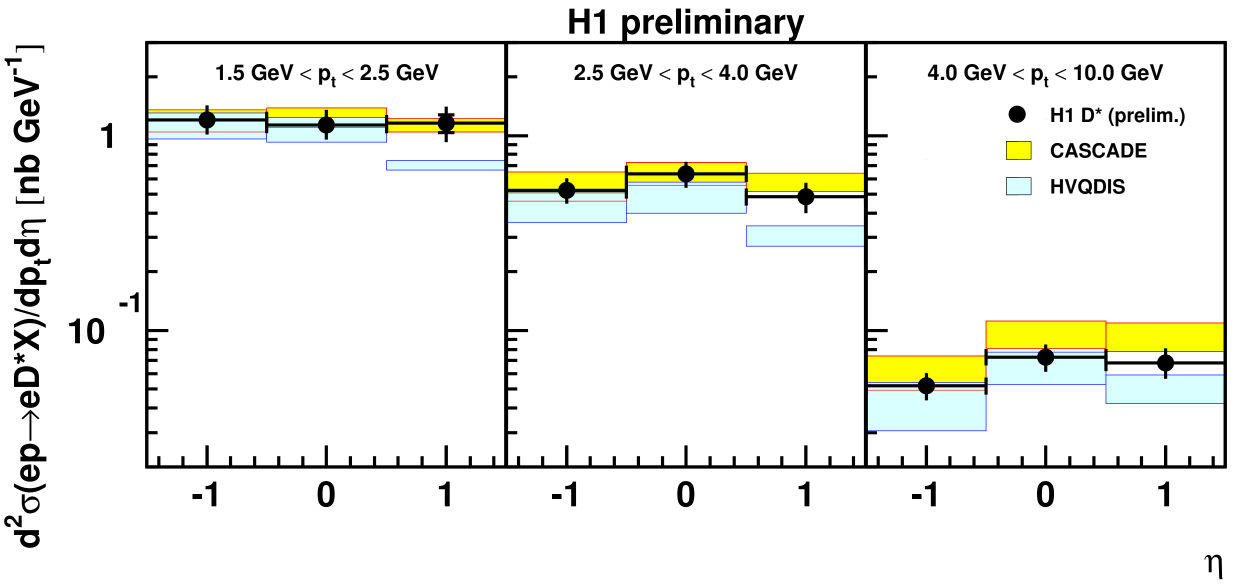

Figure 5: Double differential inclusive cross section $\mathrm{d}^2\sigma/\mathrm{d}p_{t\,D^*}\mathrm{d}\eta_{D^*}$ in bins of $p_{t\,D^*}$. The inner and outer error bars correspond to the statistical and the total errors. The data are compared to the expectations of the NLO DGLAP calculation using HVQDIS and of the CCFM calculation based on the CASCADE program (see figure 1 for details).

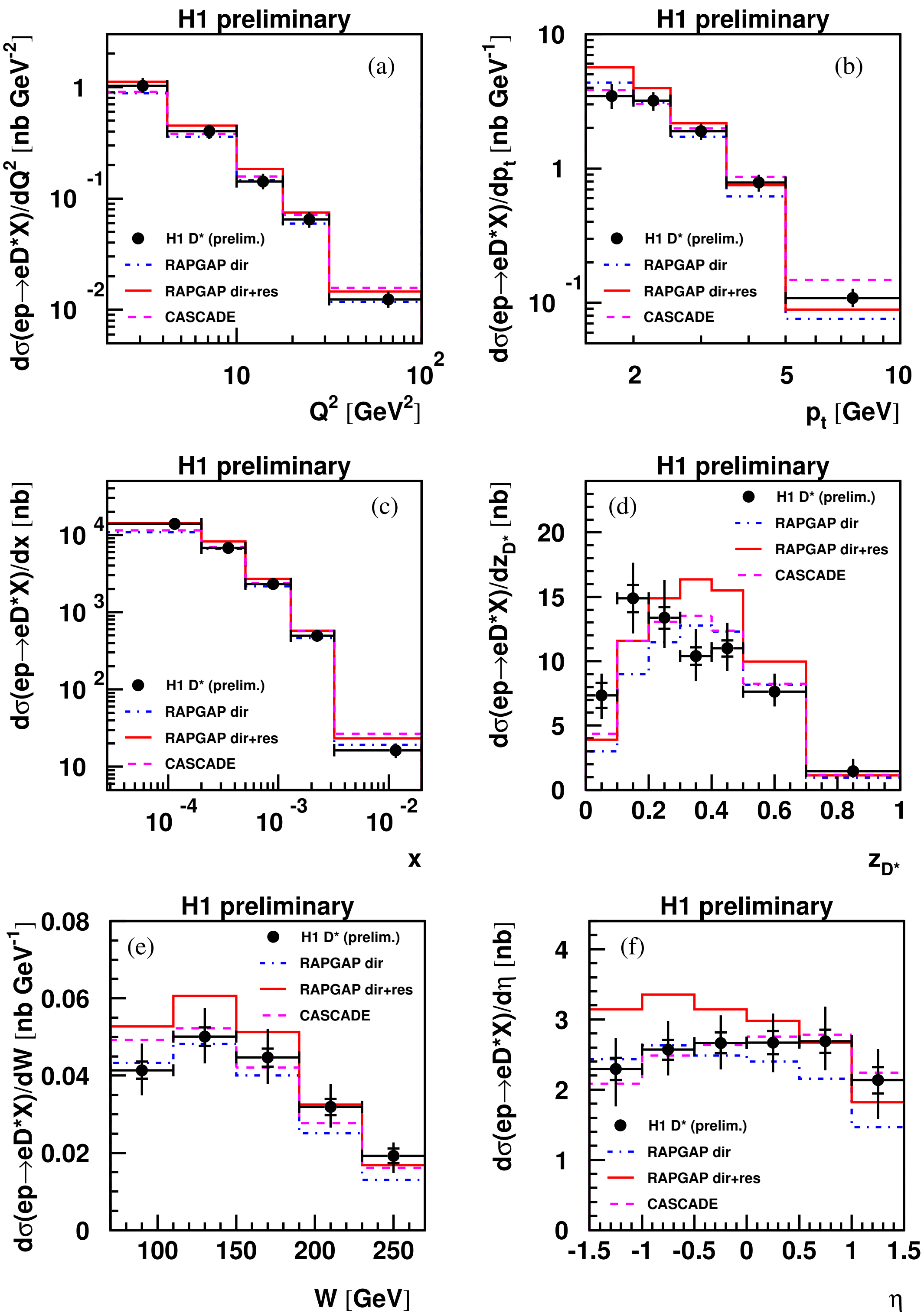

Figure 6: Single differential inclusive cross section $\sigma(ep \to eD^{*\pm}X)$ versus W, x, Q^2 and $p_{t\,D^*}$, η_{D^*}, z_{D^*}. The inner and outer error bars correspond to the statistical and the total errors. The expectation of the RAPGAP Monte Carlo (with $m_c = 1.4$ GeV, $\epsilon_c = 0.078$ and using the CTEQ5L parton density in the proton) is also shown when only direct processes are taken into account and when the resolved contribution is also considered. The expectation of the CASCADE program (with $m_c = 1.4$ GeV, $\epsilon_c = 0.078$ and the initial gluon distribution fitted to the inclusive F_2 data) is also displayed.

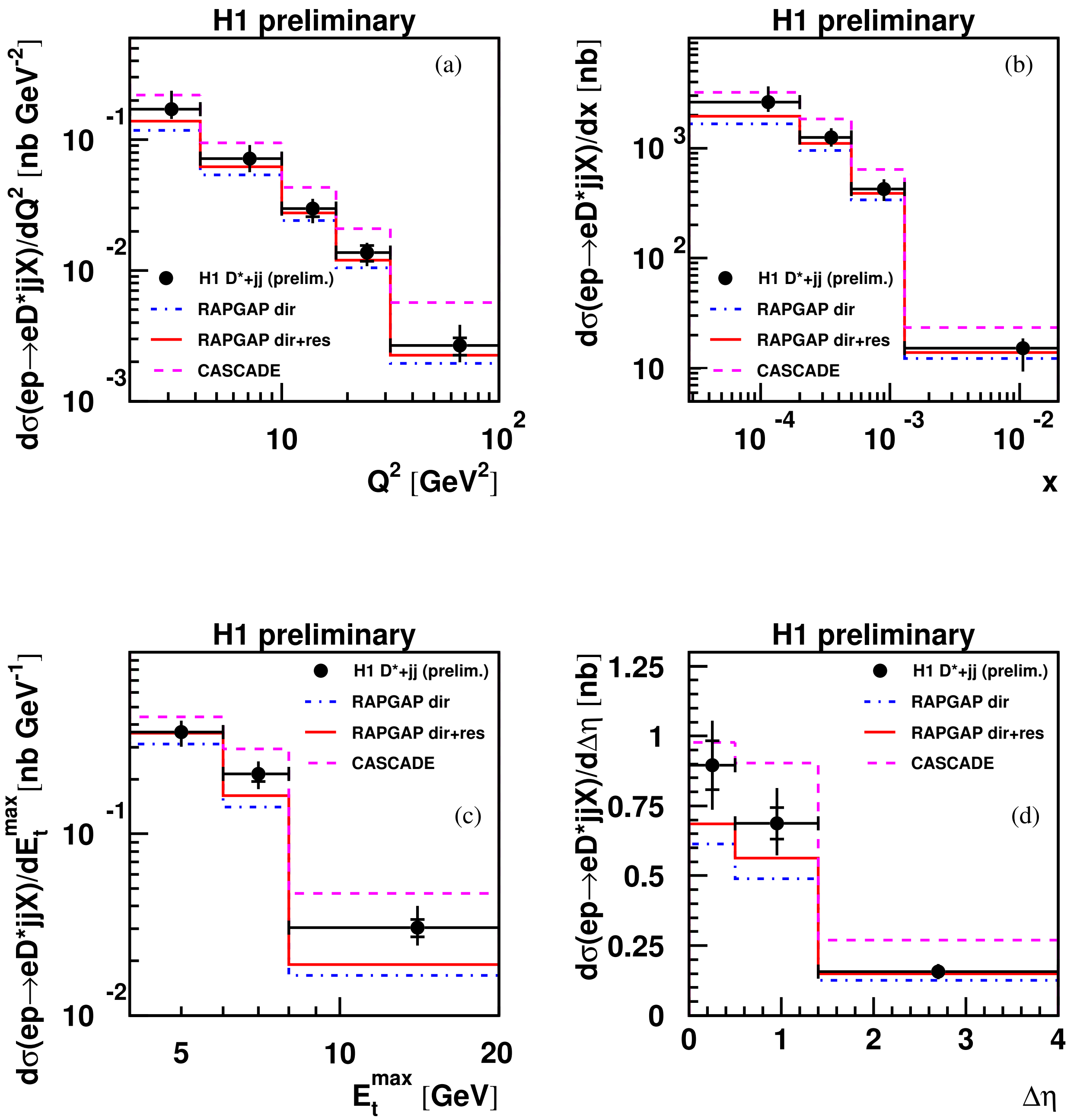

Figure 7: Dijet cross sections as a function of Q^2, x, $E_t^{\max}$ and $\Delta\eta$ for events with $D^{*\pm}$ mesons. The inner and outer error bars correspond to the statistical and the total errors. The expectation of the RAPGAP Monte Carlo (with $m_c = 1.4$ GeV, $\epsilon_c = 0.078$ and using the CTEQ5L parton density in the proton) is also shown when only direct processes are taken into account and when the resolved contribution is also considered. The data are also compared with the expectation of the CASCADE Monte Carlo with $m_c = 1.4$ GeV, $\epsilon_c = 0.078$ and the initial gluon distribution fitted to the inclusive F_2 data.

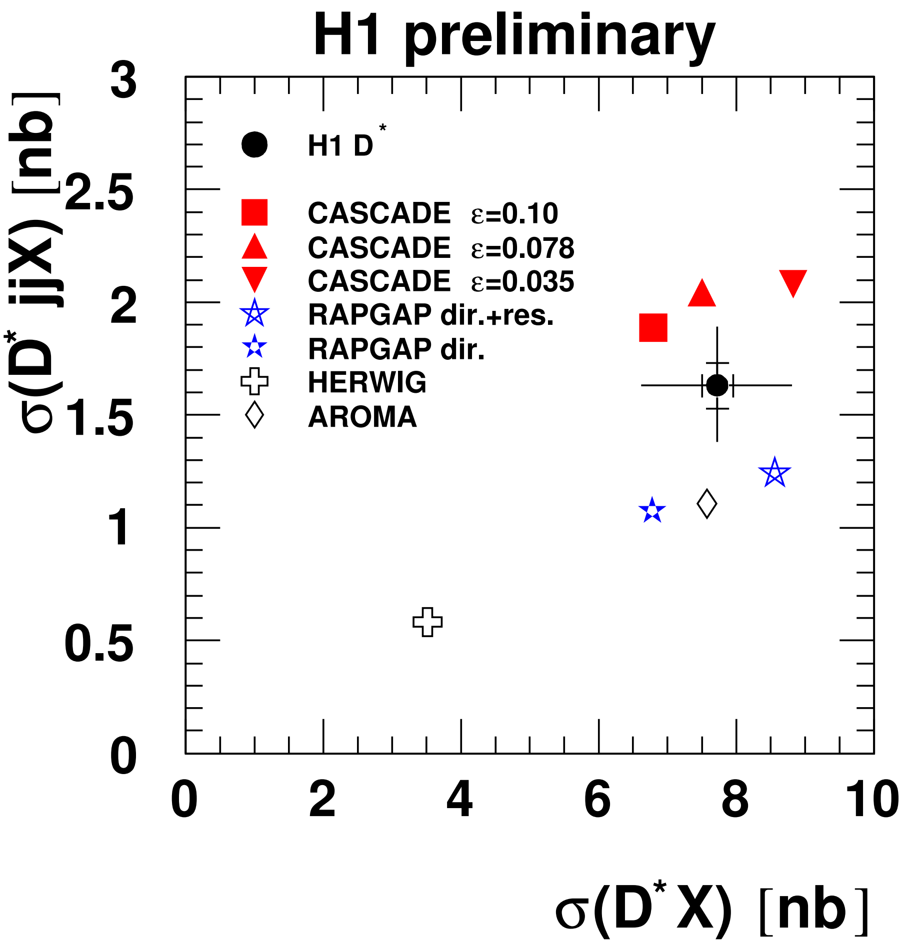

Figure 8: The cross section for associated dijet production in events with a $D^{*\pm}$ meson versus the $D^{*\pm}$ meson production cross section is shown. The expectation of the RAPGAP Monte Carlo with $\epsilon_c = 0.078$ is also shown when only direct processes are taken into account and when the resolved contribution is also considered. The predictions of the AROMA Monte Carlo with $\epsilon_c = 0.078$ and of the HERWIG Monte Carlo which uses cluster fragmentation are also displayed. For the predictions of RAPGAP, AROMA and HERWIG the charm mass $m_c = 1.4$ GeV and the CTEQ5L parton density in the proton have been used. The data are also compared with the expectation of the CASCADE Monte Carlo with the initial gluon distribution fitted to the inclusive F_2 data, for $m_c = 1.4$ GeV, $\epsilon_c = 0.078$ for $m_c = 1.3$ GeV, $\epsilon_c = 0.035$ and for $m_c = 1.5$ GeV, $\epsilon_c = 0.10$.